Effects of Deposits on Film Cooling of a Vane Endwall Along the Pressure Side

N. Sundaram
Mechanical Engineering Department,
Virginia Polytechnic Institute and
State University,
Blacksburg, VA 24061
e-mail: nasundar@vt.edu

M. D. Barringer

K. A. Thole

Mechanical and Nuclear Engineering Department,
The Pennsylvania University,
University Park, PA 16802

Film cooling is influenced by surface roughness and depositions that occur from contaminants present in the hot gas path, whether that film cooling occurs on the vane itself or on the endwalls associated with the vanes. Secondary flows in the endwall region also affect the film-cooling performance along the endwall. An experimental investigation was conducted to study the effect of surface deposition on film cooling along the pressure side of a first-stage turbine vane endwall. A large-scale wind tunnel with a turbine vane cascade was used to perform the experiments. The vane endwall was cooled by an array of film-cooling holes along the pressure side of the airfoil. Deposits having a semielliptical shape were placed along the pressure side to simulate individual row and multiple row depositions. Results indicated that the deposits lowered the average adiabatic effectiveness levels downstream of the film-cooling rows by deflecting the coolant jets toward the vane endwall junction on the pressure side. Results also indicated that there was a steady decrease in adiabatic effectiveness levels with a sequential increase in the number of rows with the deposits. [DOI: 10.1115/1.2812332]

Introduction

The flow along the endwall in a first-stage turbine vane is influenced by both roughness levels present on the surface and vortices that extend from the airfoil leading edge region to the trailing edge region. These secondary flows impact the endwall film-cooling effectiveness levels by lifting coolant jets from the endwall surface and directing them toward the vane suction side. This jet lift-off results in low adiabatic effectiveness levels along the pressure side of the vane endwall, which ultimately results in a weak layer of coolant shielding the metal hardware from the hot mainstream gases. Continuous exposure of the endwall to these extreme conditions reduces the operability and life of the hardware. The adiabatic effectiveness is a measure of the film-cooling potential along a surface downstream of the coolant injection location.

Film-cooling performance is also affected by surface deposits formed by small particles and unburned combustion products adhering to the turbine hardware. Modern gas turbines are being developed to have the capability of operating with fuels other than natural gas. Coal derived synthetic gas is one such alternative fuel, which is comparable to natural gas in terms of performance; however, it can have contaminants. The size of the contaminant particles can vary greatly from 5 μm to 60 μm [1]. While the smaller particles tend to follow the mainstream flow path, the larger particles may not due to their larger momentum and can deposit on the pressure side of the vane and endwall surfaces [2]. These larger particles when in molten form tend to quench near cooled regions on turbine component surfaces, for example, near a film-cooling hole or slot, thus leading to film-cooling depositions.

This study is aimed at understanding the effects of surface deposition and deposit location on the adiabatic effectiveness levels along the pressure side of a vane endwall. In particular, the work presented in this paper is aimed at understanding the row-by-row interaction due to depositions on the endwall surface. The effects of placing deposits upstream and downstream of single and multiple cooling hole rows were investigated.

Relevant Past Studies

A number of studies in the literature have documented the effects of using alternative fuels on the surface contamination of turbine engine components. Studies have also specifically focused on determining the effects of surface roughness and surface depositions on film-cooling performance. The current literature includes studies that have investigated the effects of using coal and other solid fuels on ash and other contaminant levels on deposition, corrosion, and erosion.

A study by Wenglarz et al. [3] showed that high levels of ash up to 40 tons/y can enter a turbine. DeCorso et al. [4] found that most coal derived fuels, even after conversion and purification, had higher levels of impurities than natural gas. They found that sulfur levels in natural gas are about 10 ppm, while for coal derived fuels the sulfur levels are approximately 1000 ppm. Moses and Bernstein [5] found that a fuel burning with 0.5% ash results in about 1.5 tons of ash per day flowing through the turbine engine. In a separate study by Wenglarz [6], it was reported that the mass fraction of the ash particles that adhere to the engine surface and contribute to deposit buildup was 0.06 with an average particle diameter of 10 μm. A recent study by Bons et al. [7] investigated the effect of ash deposits present in coal fuels using an accelerated deposition test facility. Their tests were conducted with ash particles slightly higher in mean mass diameter (13.3 μm) than those found in coal fuels. For a test duration of 3 h, they found the net particle loading to be 165 ppmw/h (parts per million by weight per hour), which resulted in an average deposit thickness of 1.3 mm.

Deposition of contaminants and other particulate matter present in the mainstream gas takes place through an impingement process in which the particles make contact with and adhere to the surface. The first row of vanes is directly subjected to the combustion products that exit the combustion chamber. This direct exposure results in an elevated level of particulate deposition via impingement [8]. The mechanism for this can be attributed to particle breakup and redistribution upon impacting the component wall surface [9]. More specifically, the leading edge film-cooling

Contributed by the International Gas Turbine Institute of ASME for publication in the JOURNAL OF TURBOMACHINERY. Manuscript received June 5, 2007; final manuscript received June 25, 2007; published online July 31, 2008. Review conducted by David Wisler. Paper presented at the ASME Turbo Expo 2007: Land, Sea and Air (GT2007), Montreal, Quebec, Canada, May 14–17, 2007.

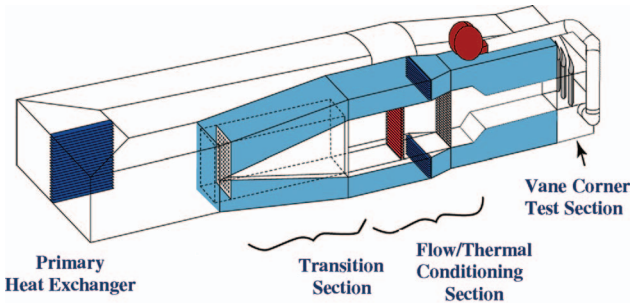

Fig. 1 Illustration of the wind tunnel facility

Table 1 Geometric and flow conditions

Scaling factor	9
Scaled up chord length (C)	59.4 cm
Pitch/Chord (P/C)	0.77
Span/Chord	0.93
Hole L/D	8.3
Re_{in}	2.1×10^5
Intel and exit angles	0 deg and 72 deg
Inlet, exit Mach number	0.017 0.085
Inlet mainstream velocity	6.3 m/s
Upstream slot width	0.024 C

regions on a turbine vane endwall are most prone to this deposition phenomenon since this is the first relatively cold surface the hot mainstream flow encounters as it enters the turbine. Bons et al. [10] showed through their turbine surface measurements that the leading edge region will have the greatest degradation. Other turbine component measurements by Taylor [11] and Tarada and Suzuki [12] revealed that all regions of a turbine blade and vane are prone to deposition and surface roughening at varying levels.

Bonding of ash and other contaminants to turbine component surfaces is also dependent on the properties of the hardware. Some studies have been performed that specifically report the effects of surface roughness on film cooling. Goldstein et al. [13] placed cylindrical roughness elements at the upstream and downstream location of film-cooling holes on a flat plate. They observed that at low blowing rates, there is a decrease in adiabatic wall effectiveness by 10–20% over a smooth surface. However, at higher blowing rates, they observed an enhancement of 40–50% in cooling performance. Schmidt et al. [14] did a similar study using conical roughness elements. They found a higher degradation of film-cooling effectiveness at lower momentum flux ratios than at higher momentum flux ratios. Barlow and Kim [15] studied the effect of a staggered row of roughness elements on adiabatic effectiveness. They found that roughness degraded cooling effectiveness compared to a smooth surface and that smaller elements caused a greater reduction than larger elements.

In addition to these studies, Cardwell et al. [16] showed that an endwall surface with uniform roughness decreased cooling effectiveness at higher blowing ratios but at lower blowing ratios there was no significant change. More recently, Sundaram and Thole [17] conducted a study to investigate the effect of localized deposition at the leading edge of a vane endwall. Their results indicated that deposits of smaller heights placed in the leading edge region enhanced the adiabatic effectiveness levels. They also found that the adiabatic effectiveness levels degraded with the increase in deposit height.

In summary, the current literature contains few studies that have focused on understanding how surface deposition affects the film-cooling performance along an endwall in a turbine. The results from this study shed some new light onto the flow physics associated with film cooling along the pressure side of turbine vane endwall and thus allow improvements to be made in endwall designs.

Experimental Methodology

The cascade test section was placed in the closed loop wind tunnel facility shown in Fig. 1. The flow encounters an elbow downstream of the fan and passes through a primary heat exchanger used to cool the bulk flow. The flow is then divided into three channels including the center passage and two cooled secondary passages located above and below the test section. Note that only the top secondary passage was used for this study. The primary core flow, located in the center passage, passes through a heater bank where the air temperature is increased to about 60°C. The secondary flow, in the outer passage, was cooled to 20°C, thereby maintaining a temperature difference of 40°C between the primary and secondary flows. The secondary flow provided the coolant through the film-cooling holes located on the endwall within the test section. For all of the tests carried out in this study, a density ratio of 1.1 was maintained between the coolant and mainstream flows. Since the density ratios were not matched to that of the engine, the velocity ratios for the cooling holes were significantly higher than those found in an engine for the same mass flux or momentum flux ratios. In this study, momentum flux ratios were set relevant to engine conditions as previous studies have shown that momentum flux ratios scale the jet lift-off well for flat plate cooling.

Downstream of the flow and thermal conditioning section is the test section that consists of two full vane passages with one center vane and two half vanes. Table 1 provides a description of the turbine vane geometry and operating conditions. The vane geometry used in the current study is a commercial first-stage vane previously described by Radomsky and Thole [18]. A detailed description of the endwall construction has been previously described by Knost and Thole [19] and Sundaram and Thole [17], who used the exact same film-cooling geometries that were used for this study. The endwall of the vane was constructed of 1.9 cm thick, low-density foam having a low thermal conductivity of 0.033 W/m K, which was mounted on a 1.2 cm thick Lexan plate. The cooling hole pattern on the endwall was cut with a five-axis water jet to ensure precision and integrity. The endwall surface was covered with 36 grit sandpaper to simulate a uniform surface roughness. The sandpaper corresponded to an equivalent sand grain roughness of 420 μm at the engine scale. In addition to the surface roughness, the endwall also simulated a combustor-turbine interface gap upstream of the vane and a vane-to-vane interface gap between the vanes. In all, the endwall used in this study simulated the geometries and surface conditions of an actual engine.

The inlet turbulence intensity and length scales were measured to be 1.3% and 4 cm, respectively. These tests were carried out at a low turbulence intensity of 1.3% to isolate the effects of deposits on endwall adiabatic effectiveness levels. For every test condition, the dimensionless pressure coefficient distribution was verified to ensure periodic flow through the passages. To set the coolant mass flow rate through the film-cooling holes, a global blowing ratio was calculated using an inviscid blowing ratio along with a global discharge coefficient C_D that was obtained from CFD studies reported by Knost and Thole [20].

Instrumentation and Temperature Measurements. A FLIR P20 infrared camera was used to spatially resolve adiabatic wall temperatures along the vane cascade endwall. Measurements were taken at six different viewing locations to ensure that the entire endwall surface was thermally mapped. The camera was placed perpendicular to the endwall surface at a distance of 55 cm from the endwall. Each picture covered an area of 24×18 cm^2, with the area being divided into 320×240 pixel locations. The spatial integration circle of the camera had a diameter equal to 0.715 mm (0.16 hole diameters). Thermocouples were also placed on the

endwall surface at different locations to directly measure the temperature and to postcalibrate the infrared images. The postcalibration process involved setting the surface emissivity at a constant value of 0.92 and the background temperature (~45°C) was then adjusted until the temperatures from the infrared images were within 0.05°C of the corresponding thermocouple data. Six camera images were taken at each of the viewing locations and an in-house MATLAB program was used to obtain a single averaged picture. The same program was also used to assemble the averaged pictures at all locations to give a complete temperature distribution along the passage endwall.

Freestream temperatures were measured at multiple locations along the vane pitch and the average was determined by using a thermocouple rake consisting of three thermocouples along the span. It was found that the variations along the pitch were less than 0.2°C and along the span they were less than 1.5°C. Voltage outputs from the thermocouples were acquired using a 32 channel National Instruments data acquisition module and a 12 bit digitizing card. All temperature data were acquired and compiled after the system reached a steady state operating condition.

The one-dimensional conduction correction method described by Ethridge et al. [21] was applied in a point-by-point manner to all adiabatic effectiveness measurements made on the endwall surface. This correction involved measuring the endwall surface effectiveness without flow passing through the film-cooling holes. This required the film-cooling holes to be blocked on the endwall in the passage under study; however, similar film-cooling flow rates were maintained through the adjacent passage to ensure the correct boundary condition was established under the endwall. The resulting correction in adiabatic effectiveness η_o was found to be 0.16 at the entrance of the vane passage for a η_{meas} value of 0.9, and 0.02 at the exit of the vane passage for a η_{meas} value of 0.2.

Experimental Uncertainty. An uncertainty analysis was performed on the adiabatic effectiveness measurements using the partial derivative method described by Moffat [22]. The precision uncertainty was determined by taking the standard deviation of six measurement sets of IR camera images with each set consisting of six images. The precision uncertainty of the measurements was found to be ±0.014°C. The bias uncertainty was ±1.0°C based on the camera specifications supplied by the manufacturer. The bias uncertainty of the thermocouples was ±0.5°C. The total uncertainty was then calculated to be ±1.02°C for the infrared images and ±0.51°C for the thermocouples. The uncertainties in the measured adiabatic effectiveness η_{meas} and the correction adiabatic effectiveness η_o were determined based on its partial derivative with respect to each temperature in the definition and the total uncertainty in the temperature measurements. The uncertainty in the measured adiabatic effectiveness was then calculated to be $\partial\eta_{meas} = \pm 0.03$ for all values of η_{meas}. Similarly, there is an uncertainty associated with the correction adiabatic effectiveness, which was estimated to be $\partial\eta_o = \pm 0.03$ at all values of η_o. Hence the total uncertainty in the adiabatic effectiveness η was calculated to be $\partial\eta = \pm 0.04$ over the entire measured range.

Test Design. The primary aim of this study was to investigate the effects of surface deposition on the adiabatic effectiveness levels along the pressure side of the vane endwall. This study was designed to examine deposition on (1) the upstream and downstream sides of the cooling hole rows, (2) a single cooling hole row, and (3) multiple cooling hole rows. The tests were conducted for three different film-cooling mass flow rates corresponding to 0.5% (M_{in}=1.6), 0.75% (M_{in}=2.3), and 0.9% (M_{in}=2.7) of the total passage mass flow rate for one vane pitch. Note that for all cases there was a 0.75% coolant flow from the upstream slot, which simulated the combustor-turbine interface gap.

Figure 2 shows a schematic of a row of film-cooling holes and the location of the upstream and downstream deposition with respect to the cooling row. Figure 2 also illustrates the cross-sectional shape of the semielliptical deposits used in this study. A detailed description of the shape and construction of the deposit was previously described by Sundaram and Thole [17]. For this study, a constant deposit height was used such that h/D=0.8 and w/D=2, where D is the film-cooling hole diameter. The deposit height was not varied in this study since Sundaram and Thole [17] showed that h/D=0.8 is representative of most results achieved for surface depositions.

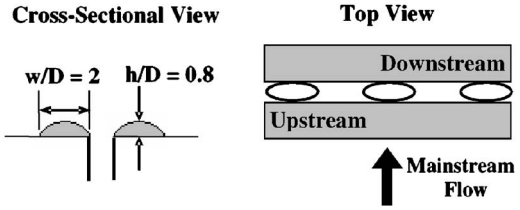

Fig. 2 Illustration of the deposit shape and geometry tested along the pressure side of the vane endwall

Figure 3 shows the film-cooling hole arrangement on the pressure side of the vane endwall. Note that these holes are aligned in the axial direction such that they inject flow directly toward the vane. Studies were conducted with single row and multiple row deposits on the first four rows of cooling holes along the vane pressure side, where each row contains three holes. The first row is located nearest to the leading edge of the vane and the fourth row is located closer to the trailing edge. The deposit on the first row will be referred to as 1R1 where the first numeral designates the number of rows that have deposits, and the second numeral designates the row in which the deposit was placed. Similarly, the single row deposit on the second film-cooling row will be referred to as 1R2, the third row as 1R3, and the fourth row as 1R4. These studies were carried out for a low film-cooling flow rate of 0.5% and a high flow rate of 0.9% through the cooling holes.

Figure 4 shows a schematic of the configuration for multiple row deposition study. This study was carried out by sequentially increasing the number of row deposits from Rows 1–4 along the

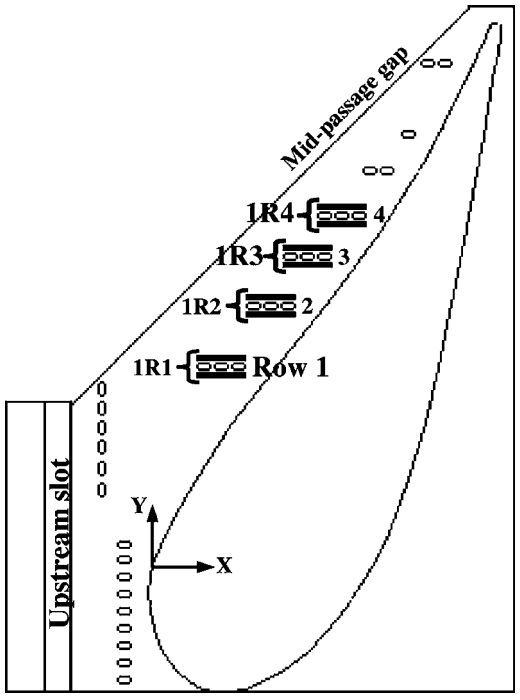

Fig. 3 Illustration of the single row deposition on the pressure side along four film cooling rows

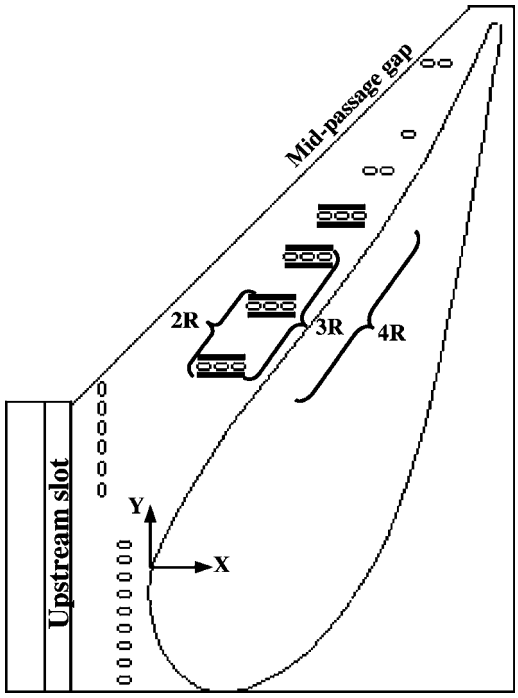

Fig. 4 Illustration of the multiple row deposition on the endwall along the pressure side

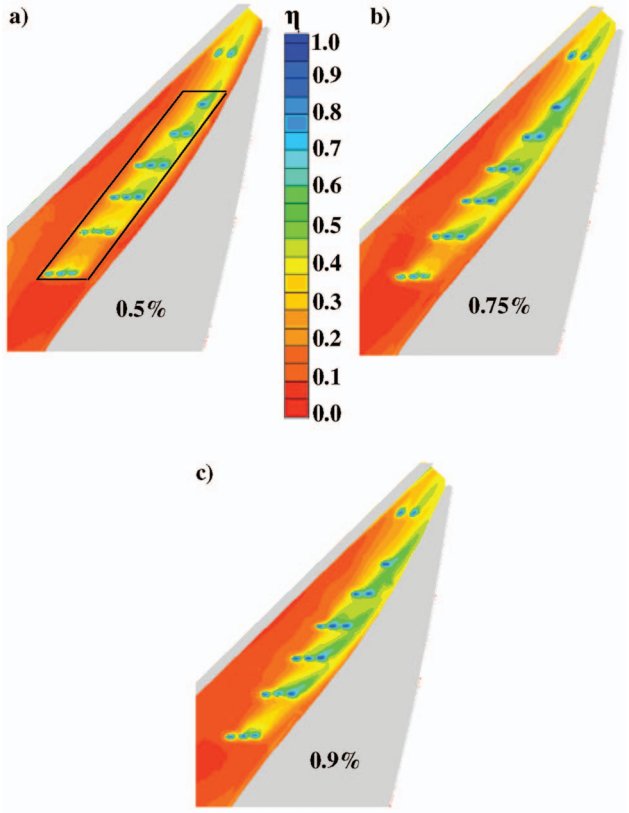

Fig. 5 Contours of adiabatic effectiveness showing the effect of increasing the film cooling mass flow rate on the pressure side for the base line study

pressure side. Deposits placed along Row 1 will be referred to as 1R, which is similar to the single row 1R1 configuration. When the deposits are placed simultaneously along Rows 1 and 2, it will be referred to as 2R. Similarly, the configuration where deposits are placed simultaneously along three and four film-cooling rows will be referred to as 3R and 4R, respectively.

Discussion of Results

Base line tests were conducted without any deposits on the pressure side of the rough endwall surface. Figures 5(*a*)–5(*c*) compare the contours of adiabatic effectiveness for the base line study with varying film-cooling flow rates. It was found that with an increase in flow rate, the adiabatic effectiveness levels increased on the pressure side. From Fig. 5(*a*), it can be seen that at a coolant flow rate of 0.5%, the coolant spreads in the direction of the mainstream passage flow. At this coolant level, the coolant exiting the film-cooling holes follows the mainstream flow path toward the suction side in spite of the coolant injection direction being toward the pressure side. As a result, there is a formation of a thin hot band along the endwall junction. With the increase in coolant flow rate to 0.75%, there is an improved streamwise spreading of the coolant resulting in an increase in the adiabatic effectiveness levels. For the 0.75% flow rate, the width of the hot band decreases in size as the coolant extends further along the endwall toward the vane-endwall junction. Further increasing the cooling flow rate to 0.9% resulted in a very small increase in adiabatic effectiveness levels with the coolant behavior being similar to the 0.75% case.

The overall effect of the cooling mass flow rate was quantified by examining the laterally averaged adiabatic effectiveness, $\bar{\eta}$. The lateral averaging was performed across the pitch in the streamwise direction within the boxed region shown in Fig. 5(*a*). Figure 6 shows the laterally averaged effectiveness for the 0.5% base line study along the pressure side. It can be seen that the effectiveness levels increase into the passage with the addition of coolant from each successive cooling row. However, downstream of Row 4 there is a decrease in $\bar{\eta}$ as the number of cooling holes in each row decreases.

Also shown in Fig. 6 is the augmentation in $\bar{\eta}$ as a result of increasing the coolant mass flow rate from 0.5% to 0.75% and 0.9%. Note that the values less than one are reductions in effectiveness levels and values greater than one are enhancements in effectiveness levels. An overall enhancement was achieved by increasing the coolant flow rate to 0.75% and a further increase to 0.9% resulted in minimal change in the enhancement levels. A flow rate of 0.9% showed higher effectiveness enhancement than 0.75% downstream of Rows 1 and 2; however, downstream of Row 3 the cooling flow rate of 0.75% showed higher effectiveness enhancement than 0.9%. This reduction in effectiveness levels

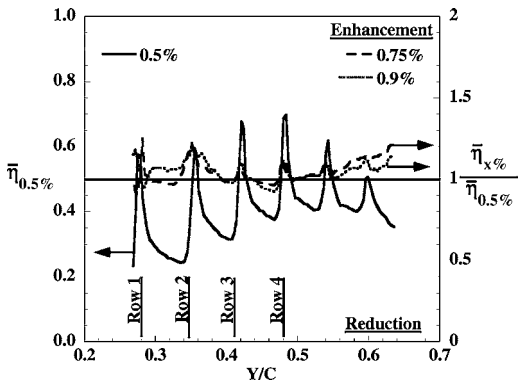

Fig. 6 Laterally averaged effectiveness for the base line study with 0.5% cooling flow rate, and enhancements in laterally averaged effectiveness for the 0.75% and 0.9% mass flow rates

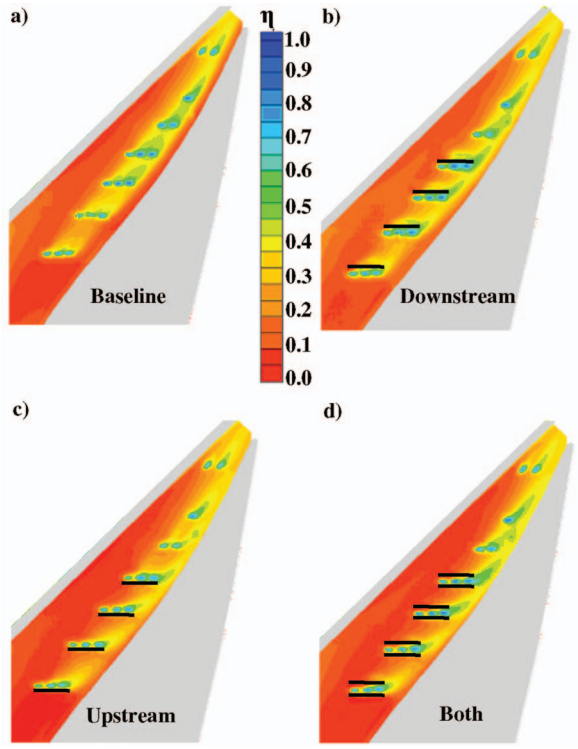

Fig. 7 Contours of adiabatic effectiveness comparing the effect of deposition at a film cooling flow rate of 0.5%

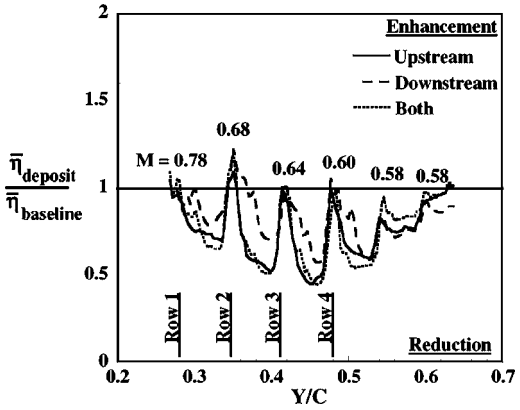

Fig. 8 Reduction in laterally averaged adiabatic effectiveness as a result of deposition located upstream, downstream, and on both sides of the cooling rows

downstream of Row 3 at 0.9% coolant flow rate is because the jets are injected at a higher trajectory leading to more mixing with the mainstream flow.

Effect of Simultaneous Multiple Row Deposits. Surface measurements made on a vane endwall by Bons et al. [10] revealed that deposition could occur at any location around the film-cooling hole. To study these effects, the base line study results were compared to cases in which the deposits were placed at the upstream side, downstream side, and both upstream and downstream sides of the cooling rows.

Figures 7(*a*)–7(*d*) compare the contours of adiabatic effectiveness levels for the three deposit configurations with the base line study. Note that deposits were simulated for the first four rows of cooling holes with a constant coolant flow rate of 0.5% through the film-cooling holes. Comparisons were made at a constant coolant flow rate of 0.5% as it is more representative of actual engine conditions. Comparing the downstream deposition shown in Fig. 7(*b*) to the base line study in Fig. 7(*a*), it is seen that this deposit configuration causes an overall reduction in adiabatic effectiveness levels. The deposit deflects the coolant jets toward the vane-endwall junction on the pressure side, which is the designed direction of the jets. The deposit acts to locally reduce the endwall cross-passage pressure gradient near the holes that would otherwise pull the coolant toward the suction surface of the adjacent vane. As the coolant flows toward the junction, there is an overall reduction in effectiveness downstream of the cooling rows.

Upstream deposition shown in Fig. 7(*c*) resulted in more coolant flowing toward the endwall junction and caused a higher reduction in effectiveness levels downstream of the cooling rows, relative to downstream deposition. Similar to these results, placing deposits on both upstream and downstream sides of the cooling rows (Fig. 7(*d*)) resulted in the bulk of the coolant becoming more confined and streamlined toward the vane-endwall junction.

From Fig. 7(*a*), it can be seen that for the base line case, the coolant from the pressure side flowed more toward the suction side resulting in higher effectiveness downstream of the holes as compared to Figs. 7(*b*)–7(*d*). Placing deposits along the pressure side cooling holes redirected the coolant toward the vane-endwall junction on the pressure side causing an overall reduction in the effectiveness levels downstream of the cooling rows.

The above effects can be further quantified by comparing the laterally averaged effectiveness. Figure 8 shows the reduction in $\bar{\eta}$ as a result of deposits located upstream, downstream, and on both upstream and downstream sides of the cooling rows. Also shown in Fig. 8 are the average local blowing ratios for each row of holes along the pressure side for a coolant mass flow rate of 0.5%. Computational predictions of the local static pressure (and local external velocity at each hole location) were used to quantify the local coolant blowing ratios from each cooling hole. It was seen that deposits upstream of the cooling rows and on both upstream and downstream sides of the cooling rows caused similar and higher degradation than deposits placed downstream of the cooling rows. As such, it can be concluded that the upstream deposits have a more dominating effect than the downstream deposits on degrading the effectiveness when the deposits are placed on both upstream and downstream sides of the cooling rows. Note that the deposits were placed on the first four cooling hole rows, but the effects are present on all the six rows. This is because in the absence of the deposits the coolant from the upstream rows adds to the effectiveness of the downstream rows, but with deposits, the coolant gets deflected toward the vane-endwall junction. This causes a reduction in effectiveness levels downstream of the coolant rows and the effect cascades to all the six rows.

An overall effect of deposits on the adiabatic effectiveness levels can be compared by using the area averaged effectiveness. Note that the area used was that shown in the box in Fig. 5(*a*). Figure 9 compares the area averaged adiabatic effectiveness levels for the different deposit configurations with the base line study for each of the three film-cooling flow rates. At a film-cooling flow rate of 0.5%, the overall effectiveness levels are the lowest for deposition on the upstream and on both sides of the cooling rows. Reduction in adiabatic effectiveness levels were seen at all the three coolant flows for the three deposit configurations, relative to the base line study. As shown earlier, the adiabatic effectiveness levels improved with an increase in coolant flow for the base line study. A similar trend in increased effectiveness levels with increased coolant flow was seen for the downstream deposition, but the overall levels were still lower than the base line study. For deposition on the upstream location and on both upstream and downstream sides of the cooling row, an increase in effectiveness levels were seen from 0.5% to 0.75%, but a further increase to 0.9% reduced the effectiveness levels. The reduction in effectiveness levels for deposits on both sides was higher than the upstream deposition at a coolant flow rate of 0.9%. Deposits on both sides showed the highest reduction in effectiveness levels and

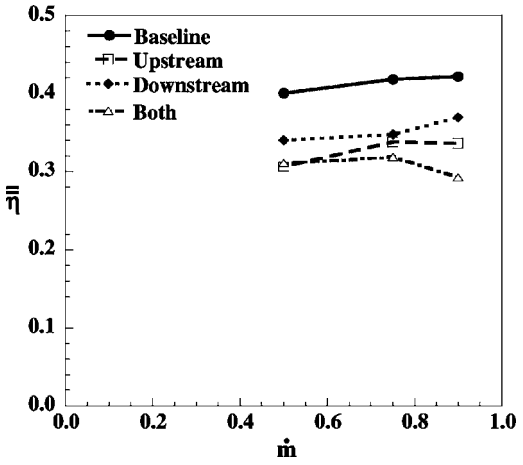

Fig. 9 Area averaged effectiveness comparing the base line study to the deposition located upstream, downstream, and both upstream and downstream

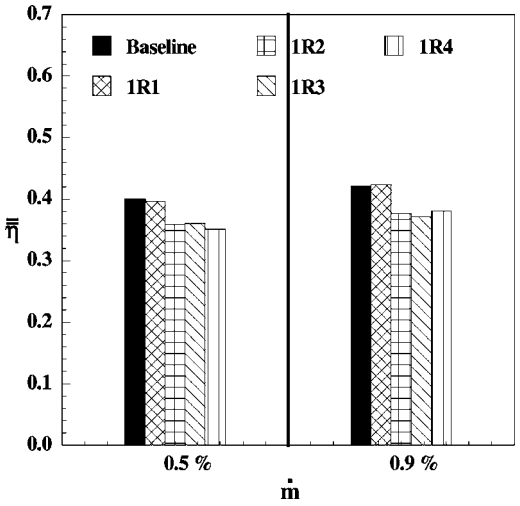

Fig. 11 Area averaged effectiveness comparing the effect of single row deposition with the base line for a low and a high film cooling flow rate

showed the combined effect of upstream and downstream depositions. As such, the configuration of placing deposits on both sides of the cooling rows was used to investigate the effects of single row and multiple row depositions.

Effect of Single Row Deposits. Tests were also performed by placing individual row deposits from Row 1 to Row 4 for film-cooling flow rates of 0.5% and 0.9%. The aim of these studies was to determine the row-to-row deposit interaction. Figure 10 compares the degradation in laterally averaged effectiveness as a result of single row deposition at a coolant mass flow rate of 0.5%. The smallest reduction in adiabatic effectiveness occurred at Row 1 for configuration 1R1. When the deposits were placed at Row 2, there was a 40% reduction caused by deposit 1R2 at that location and its effect is carried further downstream. Similarly, the local reduction in adiabatic effectiveness because of deposits 1R3 and 1R4 at location Row 3 and Row 4 was also found to be near 40%. It can be seen that at the location of the deposit there is a maximum reduction in adiabatic effectiveness levels.

The overall effect of single row deposits on the pressure side can be compared with the area averaged adiabatic effectiveness, as shown in Fig. 11. Adiabatic effectiveness values were averaged over the pressure side film-cooling rows for the area shown in Fig. 5(*a*) (boxed region). Figure 11 compares the effect of deposits with the base line study at a low coolant flow rate of 0.5% and a high coolant flow rate of 0.9%. Deposits placed in Row 1 resulted in very little effect on the overall effectiveness at both the coolant flow rates. This is explained by the fact that at Row 1 the local blowing ratio is higher than the succeeding cooling row within the passage, which results in coolant jet lift-off. As a result, the deposit at Row 1 does not deflect the coolant jets and hence there is no degradation in adiabatic effectiveness levels, Whereas the deposit configurations 1R2, 1R3, and 1R4, placed at Rows 2, 3, and 4, respectively, resulted in a similar overall degradation in effectiveness. It can be concluded that the individual effect of a single row deposit on the overall adiabatic effectiveness levels on the pressure side is independent of its location since it results in a similar overall reduction in effectiveness levels.

Effect of Sequentially Added Multiple Row Deposits. In addition to single row deposits, a study was conducted on the effects of multiple cooling row depositions along the pressure side. This was done by sequentially increasing the number of row deposits from one row (1R) to four rows (4R) along the pressure side. Figure 12 compares the degradation in laterally averaged adiabatic effectiveness with deposits placed on a single film-cooling row to those with deposits placed on two, three, and four rows at a coolant mass flow rate of 0.5%. It can be seen that the deposit at location 1R (same as deposit 1R1) has very little effect on the pressure side effectiveness levels, whereas deposit configurations 2R, 3R, and 4R have a substantial effect on lowering the effec-

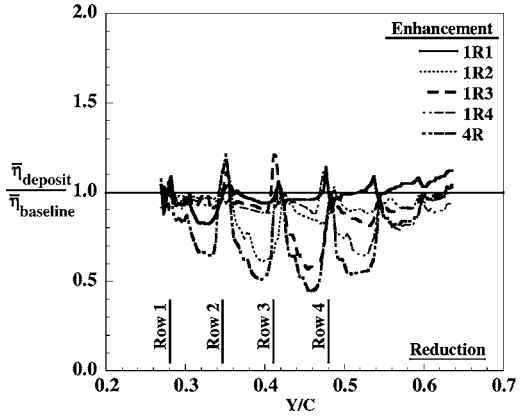

Fig. 10 Reduction in laterally averaged effectiveness as a result of single row deposits located along the pressure side at a coolant flow rate of 0.5%

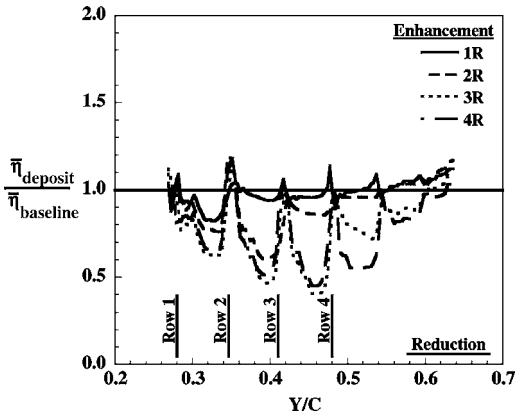

Fig. 12 Reduction in laterally averaged effectiveness as a result of sequentially added multiple row deposits on the pressure side at a coolant flow rate of 0.5%

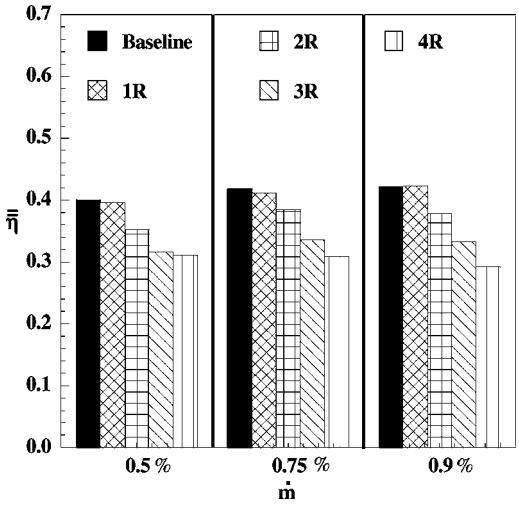

Fig. 13 Area averaged effectiveness comparing the effect of multiple row deposition with the base line for a low and a high film cooling flow rate

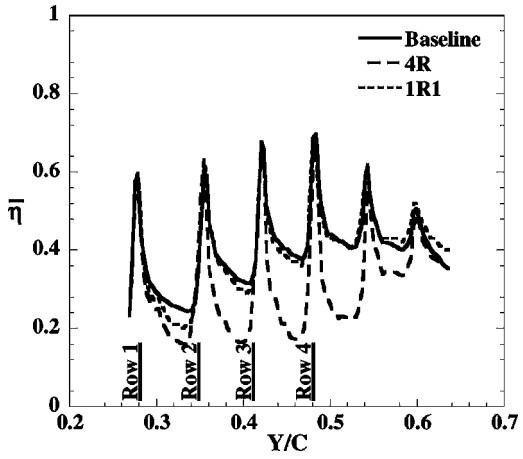

Fig. 14 Comparison of $\bar{\eta}$ between the base line and cases 1R1 and 4R (film cooling at 0.5%)

tiveness levels downstream of the film-cooling holes. Sequentially increasing the number of deposits rows had a cascading effect on lowering the effectiveness levels.

The overall result of multiple row deposits was further quantified by comparing the area averaged effectiveness levels along the pressure side. Figure 13 compares the effect of increasing the number of deposit rows with the base line study at coolant mass flow rates of 0.5%, 0.75%, and 0.9%. At the low mass flow rate of 0.5%, there is a reduction of 10% in effectiveness levels with the successive increase in the number of deposit rows from 1R to 3R. There was only a slight continued reduction in effectiveness levels from changing the deposit configuration from 3R to 4R. At the high flow rate of 0.9%, there was a near linear reduction of 10% in the area averaged effectiveness levels with a sequential increase in the number of row deposits. Note that the trends shown at the coolant flow rate of 0.75% were consistent with the high coolant flow rate of 0.9%. Multiple row deposits on the endwall were found to have a detrimental effect on the effectiveness levels along the pressure side. This multiple row deposition is most likely what occurs in an actual engine.

Superposition of Deposits. An overall comparison of the laterally averaged adiabatic effectiveness between the base line study, single row deposition study (1R1), and the multiple row deposition (4R) study is shown in Fig. 14 at a film-cooling flow rate of 0.5%. The question of whether or not the results from the four row deposit study (4R) can be accurately predicted by superimposing the results from single rows of deposits is an important one. Two superposition approaches were considered to determine if the results from a single hole row were cumulative.

The first method involved using the superposition method developed by Sellers [23] to predict the overall reduction in $\bar{\eta}$ due to multiple row deposition. The reduction in $\bar{\eta}$ at the first film-cooling row due to a single row deposit was calculated to be $\Delta\bar{\eta}_{1R1}=\bar{\eta}_{\text{baseline}}-\bar{\eta}_{1R1}$. Similarly, reductions along Rows 2, 3, and 4 were calculated to be $\Delta\bar{\eta}_{1R1}$, $\Delta\bar{\eta}_{1R3}$, and $\Delta\bar{\eta}_{1R4}$, respectively. Using the above single row reductions in adiabatic effectiveness, the overall reduction in adiabatic effectiveness $\Delta\bar{\eta}_{\text{overall}}$ was calculated by applying the method developed by the Sellers [23]. Then the predicted result was simply $\Delta\bar{\eta}_{4R}=\bar{\eta}_{\text{baseline}}-\Delta\bar{\eta}_{\text{overall}}$ and the result is shown in Fig. 15. It can be seen that this method resulted in overpredicting the degradation in $\bar{\eta}$ at each film-cooling hole row by about 40%.

The second superposition method involved using the reduction in $\bar{\eta}$ from the base line due to adding a single row of deposits at each individual corresponding row of film-cooling holes. This resulted in a prediction of the form $\Delta\bar{\eta}_{4R}=\bar{\eta}_{\text{baseline}}-\Delta\bar{\eta}_{1R1}-\Delta\bar{\eta}_{1R2}-\Delta\bar{\eta}_{1R3}-\Delta\bar{\eta}_{1R4}$ and the results are also shown in Fig. 15. It can be seen that this second method also resulted in overestimating the reduction in $\bar{\eta}$ and the error at each film-cooling row was about 40% similar to Method 1.

This study indicates that there is not a linear cumulative effect in adding the reduction in resulting from the single row of deposits in order to predict the results when multiple rows of deposits are present. This is due to the fact that there is a varied effect that the deposits at the downstream hole row have on adiabatic effectiveness levels at the upstream hole rows. The degrading effect on the adiabatic effectiveness levels at the upstream hole row due to deposits on the downstream hole row is contingent upon the simultaneous presence of a deposit at the upstream location. This effect violates most superposition methods and hence there is a discrepancy between the predicted and measured adiabatic effectiveness levels. Another important result is that from viewing Figs. 10, 12, and 14, it can be seen that the third row was the row that was most affected by the presence of the deposits in both the single row configurations and the multiple row configurations.

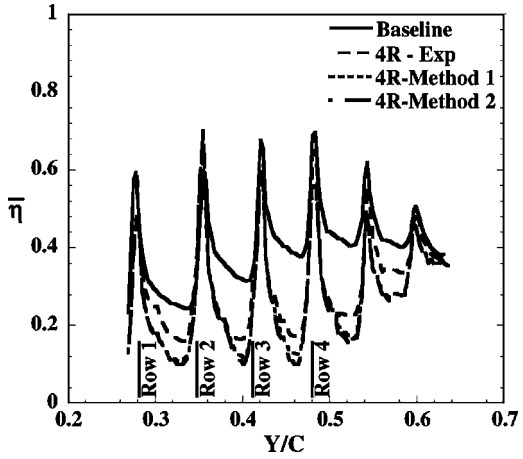

Fig. 15 Comparison of two superposition methods in predicting the results for the four row deposition study (film cooling at 0.5%)

Conclusions

Measurements of adiabatic effectiveness levels were presented on a turbine vane endwall with simulated surface depositions. The depositions were studied along the pressure side of the endwall, and were placed upstream, downstream, and on both sides of four rows of film-cooling holes. The focus of this paper was on evaluating the effect of single row, multiple row, and sequentially added deposits to the overall reductions that would occur for endwall film cooling. The effect of the deposits on endwall adiabatic effectiveness levels was compared with a base line study having no surface deposition.

It was found that deposition upstream and on both the upstream and downstream of the cooling holes resulted in similar and higher degradation in effectiveness levels than deposition located just downstream of the cooling holes. When using deposits on both the upstream and downstream regions of the cooling holes, the effect of a single row deposition was investigated. The single row deposits resulted in similar degradation of the total area averaged effectiveness that was independent of row location, with the exception of the first row, which showed little degradation.

Sequentially increasing the number of deposition rows resulted in a significant decrease in the overall adiabatic effectiveness levels. The results indicate that there is a linear reduction in adiabatic effectiveness levels with the sequential increase in the number of row deposits. This effect is more prominent at the higher coolant flow rate of 0.9% than at the lower flow rate of 0.5%.

Finally, the work presented in this paper indicates that by applying superposition methods the degradation in adiabatic effectiveness can be predicted within a 40% error. The overprediction using superposition occurs because of the large effect that the downstream deposits can have on upstream rows when deposits are placed along multiple rows.

Acknowledgment

This publication was prepared with the support of the US Department of Energy, Office of Fossil Fuel, and National Energy Technology Laboratory. Any opinions, findings, conclusions, or recommendations expressed herein are solely those of the authors and do not necessarily reflect the views of the DOE. The authors thank Mike Blair (Pratt & Whitney), Ron Bunker (General Electric), and John Weaver (Rolls-Royce) for their input on the modeling of realistic turbine features.

Nomenclature

- C = true chord of stator vane
- D = diameter of film-cooling hole
- h = height of the deposit
- L = film-cooling hole length
- M_{in} = blowing ratio based on inlet mainstream velocity $M_{in}=\rho_j U_j/\rho_{in}U_{in}$
- $\dot{m}$ = coolant mass flow rate
- P = vane pitch, hole pitch
- PS = pressure side
- Re_{in} = Reynolds number defined as $Re_{in}=CU_{in}/\nu$
- S = span of stator vane
- T = temperature
- U = velocity
- w = width of the deposit
- X,Y,Z = local coordinates

Greek

- η_{meas} = measured adiabatic effectiveness, $\eta_{meas}=(T_\infty - T_{meas})/(T_\infty - T_J)$
- η_o = correction adiabatic effectiveness
- η = adiabatic wall effectiveness, $\eta=(\eta_{meas}-\eta_o)/(1-\eta_o)$
- $\bar{\eta}$ = laterally averaged effectiveness
- $\bar{\bar{\eta}}$ = area-averaged effectiveness
- ν = kinematic viscosity

Subscripts

- aw = adiabatic wall
- in = inlet conditions
- j = coolant flow through film-cooling holes
- ∞ = local freestream conditions

References

[1] Bons, J. P., Crosby, J., Wammack, J. E., Bentley, B. I., and Fletcher, T. H., 2005, "High Pressure Turbine Deposition in Land Based Gas Turbines From Various Synfuels," ASME Paper No. GT2005-68479.

[2] Wenglarz, R. A., 1985, "Deposition, Erosion, and Corrosion Protection for Coal-Fired Gas Turbines," ASME Paper No. 85-IGT-61.

[3] Wenglarz, R. A., Nirmalan, N. V., and Daehler, T. G., 1995, "Rugged ATS Turbines for Alternate Fuels," ASME Paper No. 95-GT-73.

[4] Decorso, S. M., Newby, R. A., Anson, D., Wenglarz, R. A., and Wright, I. G., 1996, "Coal/Bimass Fuels and the Gas Turbine: Utilization of Solid Fuels and Their Derivatives," ASME Paper No. 96-GT-76.

[5] Moses, C. A., and Bernstein, H. L., 1996, "Fuel-Specification Considerations for Biomass Pyrolysis Liquids to be Used in Stationary Gas Turbines," ASME Paper No. 96-GT-406.

[6] Wenglarz, R. A., 1992, "An Approach for Evaluation of Gas Turbine Deposition," ASME J. Eng. Gas Turbines Power, **114**, pp. 230–234.

[7] Bons, J. P., Corsby, J., Wammack, J. E., Bentley, B. I., and Fletcher, T. H., 2005, "High Pressure Turbine Deposition in Land Based Gas Turbines From Various Synfuels," ASME Paper No. GT2005-68479.

[8] Bornstein, N. S., 1996, "Reviewing Sulfidation Corrosion—Yesterday and Today," J. Minerals, Metals, and Materials Society, **48**(11), pp. 37–39.

[9] Wright, I. G., Leyens, C., and Pint, B. A., 2000, "An Analysis of the Potential for Deposition, Erosion, or Corrosion in Gas Turbines Fueled by the Products of Biomass Gasification or Combustion," ASME Paper No. 2000-GT-0019.

[10] Bons, J. P., Taylor, R. P., McClain, S. T., and Rivir, R. B., 2001, "The Many Faces of Turbine Surface Roughness," ASME J. Turbomach., **123**, pp. 739–748.

[11] Taylor, R. P., 1990, "Surface Roughness Measurements on Gas Turbine Blades," ASME J. Turbomach., **112**, pp. 175–180.

[12] Tarada, F., and Suzuki, M., 1993, "External Heat Transfer Enhancement to Turbine Blading Due to Surface Roughness," ASME Paper No. 93-GT-74.

[13] Goldstein, R. J., Eckert, E. R. G., and Chiang, H. D., 1985, "Effect of Surface Roughness on Film Cooling Performance," ASME J. Eng. Gas Turbines Power, **107**, pp. 111–116.

[14] Schmidt, D. L., Sen, B., and Bogard, D. G., 1996, "Effects of Surface Roughness on Film-Cooling," ASME Paper No. 96-GT-299.

[15] Barlow, D. N., and Kim. Y. W., 1995, "Effect of Surface Roughness on Local Heat Transfer and Film Cooling Effectiveness," ASME Paper No. 95-GT-14.

[16] Cardwell, N. D., Sundaram, N., and Thole, K. A., 2005, "Effects of Mid-Passage Gap, Endwall Misalignment, and Roughness on Endwall Film-Cooling," ASME J. Turbomach., **128**, pp. 62–70.

[17] Sundaram, N., and Thole, K. A., 2006, "Effects of Surface Deposition, Hole Blockage, and Thermal Barrier Coating Spallation on Vane Endwall Film-Cooling," ASME J. Turbomach., **129**, pp. 599–607.

[18] Radomsky, R., and Thole, K. A., 2000, "Flowfield Measurements for a Highly Turbulent Flow in a Stator Vane Passage," ASME J. Turbomach., **122**, pp. 255–262.

[19] Knost, D. G., and Thole, K. A., 2004, "Adiabatic Effectiveness Measurements of Endwall Film Cooling for a First Stage Vane," ASME J. Turbomach., **127**, pp. 297–305.

[20] Knost, D. G., and Thole, K. A., 2003, "Computational Predictions of Endwall Film Cooling for a First Stage Vane," ASME Paper No. GT2003-38252.

[21] Ethridge, M. I., Cutbirth, J. M., and Bogard, D. G., 2000, "Scaling of Performance for Varying Density Ratio Coolants on an Airfoil With Strong Curvature and Pressure Gradient Effects," ASME J. Turbomach., **123**, pp. 231–237.

[22] Moffat, R. J., 1988, "Describing the Uncertainties in Experimental Results," Exp. Therm. Fluid Sci., **1**, pp. 3–17.

[23] Sellers, J. P., 1963, "Gaseous Film Cooling With Multiple Injection Stations," AIAA J., **1**, pp. 2154–2156.